Hybrid numerical 3D model of electromagnetic levitation of molten metal

Slawomir Golak[a], Christophe Geuzaine[b], Roman Przylucki[a], Blazej Nycz[a], Francois Henrotte[b]

[a] *Silesian University of Technology, Faculty of Materials Engineering, Department of Industrial Informatics, Katowice, Poland*
[b] *University of Liège, Faculty of Engineering, Department of Electrical Engineering and Computer Science, Liège, Belgium*

Abstract

This paper introduces a new and efficient methodology for the numerical modeling of electromagnetic levitation. The model requires transferring the time-varying geometry of the molten metal from the hydrodynamic submodel to the electromagnetic submodel. The developed methodology combines a geometry transfer of the conductivity distribution of the metal/air system, and the accompanying conditional reconstruction of the electromagnetic submodel. The proposed solution strategy enables a computationally efficient simulation of the coupled process accounting for any evolution of the molten metal geometry. The developed methodology can be generalized to any magnetohydrodynamic process with the presence of a free surface of liquid metal. The method was applied to the 3D modeling of a classic example of low-scale levitation melting of aluminum.

Keywords: electomagnetic leviation melting, numerical modeling, magnetohydrodynamics (MHD)

1. Introduction

Metal levitation melting enables the processing of highly reactive or high purity metals [1, 2, 3, 4, 5]. Contact of such materials with a crucible may cause damage, corrosion of the container and contamination of the metal itself [6, 7, 8]. The levitational melting process has been invented in the 1920s, and after years of stagnation, it has undergone in the recent years a visible progress due to the increase in the technical importance of metal alloys

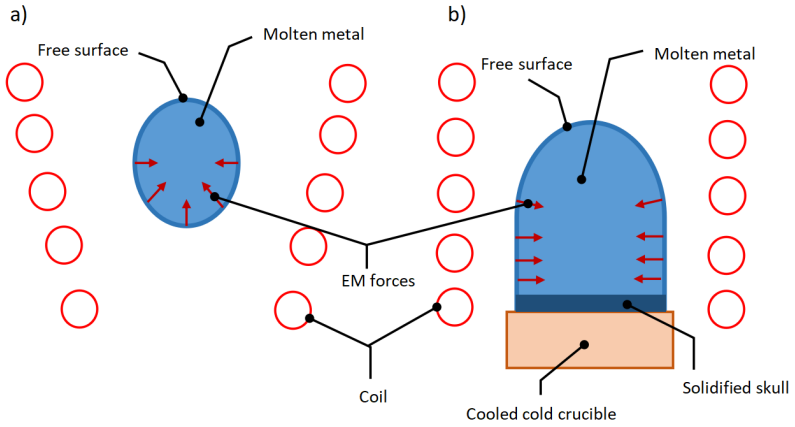

Figure 1: Simplified scheme of full levitation melting (a) and semi-levitation melting (b)

with high reactivity or very high purity. In the case of fully levitation melting (Fig. 1a), in which the molten metal has no contact with the device, design solutions have finally appeared that enable melting of metal loads weighing more than several dozen grams [9, 10, 11]. Even greater progress towards industrial applications can be observed for the semi-levitation process using a cold crucible (Fig. 1b). In this process, thanks to the mechanical support of the molten metal bath through a layer of solidified metal (so-called skull, produced by contact with the cooled cold crucible), one is able to melt loads weighing several kilograms. For this type of levitation melting, intensive research is carried out in terms of modeling, increasing the efficiency of this process and the degree of superheating of the molten metal (heating above the melting point) [12, 13, 14, 15, 16, 17]. In processes like levitation melting, semi-levitation melting in a cold crucible, melting of metals in non-conductive crucibles [18], and all processes [19] dealing with a free surface of liquid metal in the presence of an electromagnetic field, a strong coupling coupling must be realized between the hydrodynamic submodel and electromagnetic submodel. However, due to the low values of the magnetic Reynolds number Re_m, the direct influence of the flow velocity field can be omitted in such a coupling.

There are many computational models for this class of problems. If the shape and position of the molten metal is known, based on experimental measurements for instance, it is enough to transfer the distributions of metal temperatures, Lorentz forces and Joule heat sources between the hydrodynamic and the electromagnetic model [20]. However, this approach cannot

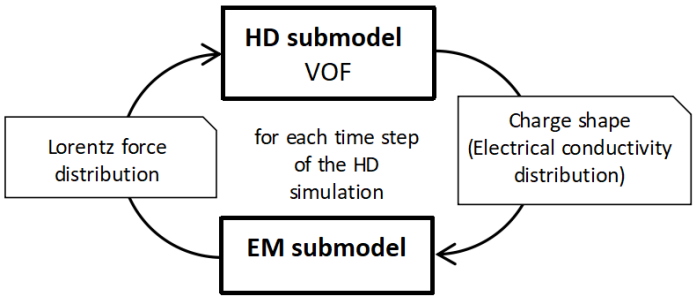

Figure 2: Diagram of a levitation melting simulation cycle

be directly used to design a new electromagnetic levitation device, including the coil geometry and power supply parameters. For such applications, it is necessary to take into account the flow-induced shape change of the liquid metal region. This is because changes in the shape of the liquid metal cause changes in the distribution of the electromagnetic field and therefore changes in the position of the load equilibrium point for gravity and electromagnetic forces. Reciprocally, the Lorentz forces generated by this field change the shape of the metal. Therefore, both fields (hydrodynamic HD and electromagnetic EM) must be coupled in this regard during the process simulation. The hydrodynamic simulation plays the primary role in standard methodologies (Fig. 2). At each time step, the current shape of the metal is determined and transferred to the electromagnetic submodel, which then calculates and returns the distribution of Lorentz forces acting on the liquid metal. These forces modify the shape of the metal load, and the simulation cycle starts again. The problem is the maximum time step size of the parent hydrodynamic simulation. In order to ensure a proper tracking of the metal/air interface, the time step cannot be larger than 0.01 s, and in case of more dynamic changes, it must be reduced down to 0.0001 s [21, 22, 13, 14] (to maintain low Courant number which is required by the multiphase solver). At each time step, the EM submodel evaluates a new distribution of the electromagnetic field over the entire domain (surroundings, coil, molten metal) to determine the Lorentz forces. Therefore, electromagnetic calculations are the bottleneck of the coupled simulation process, and ways to increase the simulation efficiency should be sought in the EM model. In the existing literature on the subject, we can identify two main approaches.

The first approach consists in representing explicitly the liquid metal sur-

face with appropriate geometric parameters (e.g. characteristic points) and in creating an updated geometry, as well as a new mesh of the electromagnetic model, at each time step of the hydrodynamic simulation [21, 23, 17]. This approach reduces the efficiency of the simulation system due to the numerical cost of repeatedly generating a new EM model mesh, and the induced difficulty to reuse the electromagnetic field solution from the previous time step. This is a big waste if we take into account the fact that the EM field distributions in adjacent time steps only differ slightly. Moreover, a solution based on a geometric representation of the shape of the metal region has limitations in terms of complexity, in case of the presence of gas bubbles in the liquid metal area for instance.

The second approach is based on using a fixed mesh for the electromagnetic model. The shape of the liquid metal is transferred from the hydrodynamic model to the electromagnetic model by transferring the electrical conductivity distribution mapping this shape [13, 14, 15, 16]. The advantage of this method is a simple and automatic transfer of load shapes with any level of complexity. Moreover, it makes it possible to reuse the EM field solution from the previous time step in the current time step. Finally, in the area where the metal/air phase system is present, coherent meshes can be used in the EM model and in the HD model, which avoids inaccuracies caused by interpolation. Unfortunately, as the frequency of the electromagnetic field increases, it becomes necessary to increase the mesh density in the area of potential presence of liquid metal (due to the decrease in the field penetration depth). If the frequency is high and the ratio of the volume of the area of potential presence of liquid metal to the volume of this metal is large (as in the example analyzed in this paper), this second approach becomes very ineffective.

Due to the shortcomings of both approaches, a hybrid solution is proposed in this paper. The idea is to work with a fixed EM model mesh, consistent with the HD model mesh, but covering only a close vicinity of the current position of the liquid metal. This mesh is rebuilt only when the liquid metal leaves the area of the dense mesh.

The proposed hybrid approach offers the benefits of the fixed mesh approach, avoiding mesh generation at each simulation time step and exploiting the electromagnetic field solution from the previous time step (limitations of the variable mesh approach). At the same time, compared to the classic solution with a fixed mesh, it allows to limit the global number of nodes to a number comparable to the approach based on a variable mesh. Limiting the

frequency of mesh generation, using data from previous time steps by the proposed preconditioner preservation strategy while optimizing the number of mesh nodes allowed for a reduction in the computational cost.

The developed methodology is applicable to any MHD process involving a free surface of liquid metal. In this paper the method is demonstrated by modeling a classic example of small-scale levitational aluminum melting, which is a challenging application example.

2. Model of the electromagnetic levitation

The core of the developed 3D model is based on the shape transfer of liquid metal through conductivity distribution. According to (1), the electrical conductivity σ_{shape} transferred to the HD submodel is a function of the volume fraction of the metal phase α_{metal}:

$$\sigma_{shape} = \alpha_{metal} * \sigma_{metal} + \epsilon \tag{1}$$

where α_{metal} is the volume fraction of the metal phase, σ_{metal} is the electrical conductivity of molten metal and ϵ is a small value to ensure numerical stability.

More customizable electromagnetic simulation software allows for introducing a non-uniform conductivity distribution into the model. One such tool is the GetDP [24, 25] software used by the authors, which provides great flexibility in co-creating various simulation systems. This software has an additional important feature that increases the performance of the coupled simulation. It allows reusing results from previous time steps, in particular the matrix preconditioners used to speed up the convergence of the linear solvers. The diagram in Fig. 3 shows the simulation cycle performed on the side of the EM submodel implemented in GetDP.

At start-up, the EM submodel loads the geometry of the system with the initial position of the molten metal and its close surroundings. Then Gmsh [26] (the mesher for GetDP) generates the mesh. A dense mesh is generated in the surroundings of the liquid metal in order to resolve the small penetration depth of the high-frequency electromagnetic field. In the next step, GetDP initializes the model.

Then a preconditioner is created (using LU Factorization in our model). This matrix allows transforming the original system of equations into one with a more favorable condition number. The condition number of the

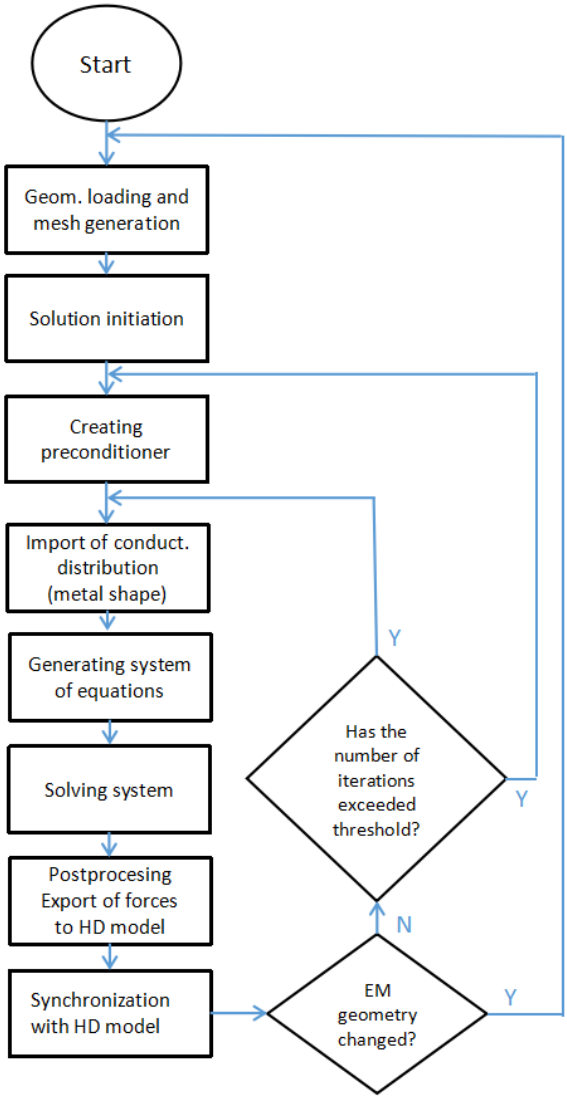

Figure 3: Simulation cycle performed by the EM submodel (implemented in Gmsh/GetDP software)

system heavily influences the speed of convergence of the iterative Krylov subspace method (typically GMRES [27]) used to solve the linear systems. Therefore, the ideal preconditioner matrix should yield a significantly lower condition number compared to the original system matrix. By recalculating the preconditioner (which can be computationally expensive) less often, the calculation time of the EM submodel can be significantly shortened.

Next the EM model imports the shape of the liquid metal from the HD model (implemented in Ansys Fluent) in the form of an electrical conductivity distribution (1).

In the next step, a system of equations is solved iteratively. After solving the system, post-processing determines the distribution of Lorentz forces acting on the liquid metal, which is transferred to the hydrodynamic submodel (Fluent). Then, the EM submodel waits for the HD submodel to use the computed force distribution and for the decision of the superior hydrodynamic cycle (Fig. 2) on whether to rebuild or not the EM model geometry. In case of mesh rebuild, the EM solution of the previous step cannot be reused as an initial solution for the GMRES iterations and the preconditioner has to be recomputed. Otherwise, the number of GMRES iterations in the previous time step of EM calculations is checked. If it exceeds a chosen threshold, the stored preconditioner is considered no longer accurate enough, and it is reevaluated.

The decision to rebuild the EM model geometry is based on the detection of the liquid metal crossing the margin line of the high mesh density area. In Fig. 4, this margin boundary is marked with a dashed line (in the EM model). If the liquid metal (after determining its new position and shape) enters the margin area, the HD submodel transmits commands to the EM submodel to change the geometry along with shifting the high-density mesh area towards the violation (the green arrow). As can be seen in the figure, the absolute position in space of the metal does not change, but thanks to this shift of the high-density area, the entire metal bath is again outside the margin area. If the metal load was deformed so that the margins on both sides of this area were violated, the high-density area would be enlarged instead of shifted, but the principle and result would be the same. The metal bath will again be in the center of the high-density area, inside the zone defined by the margins. This procedure causes the EM model to dynamically focus its attention on the molten metal area. Thanks to this, we limit the increased density of mesh nodes only to this area and reduce the global number of mesh nodes of the EM model, thus accelerating calculations. The

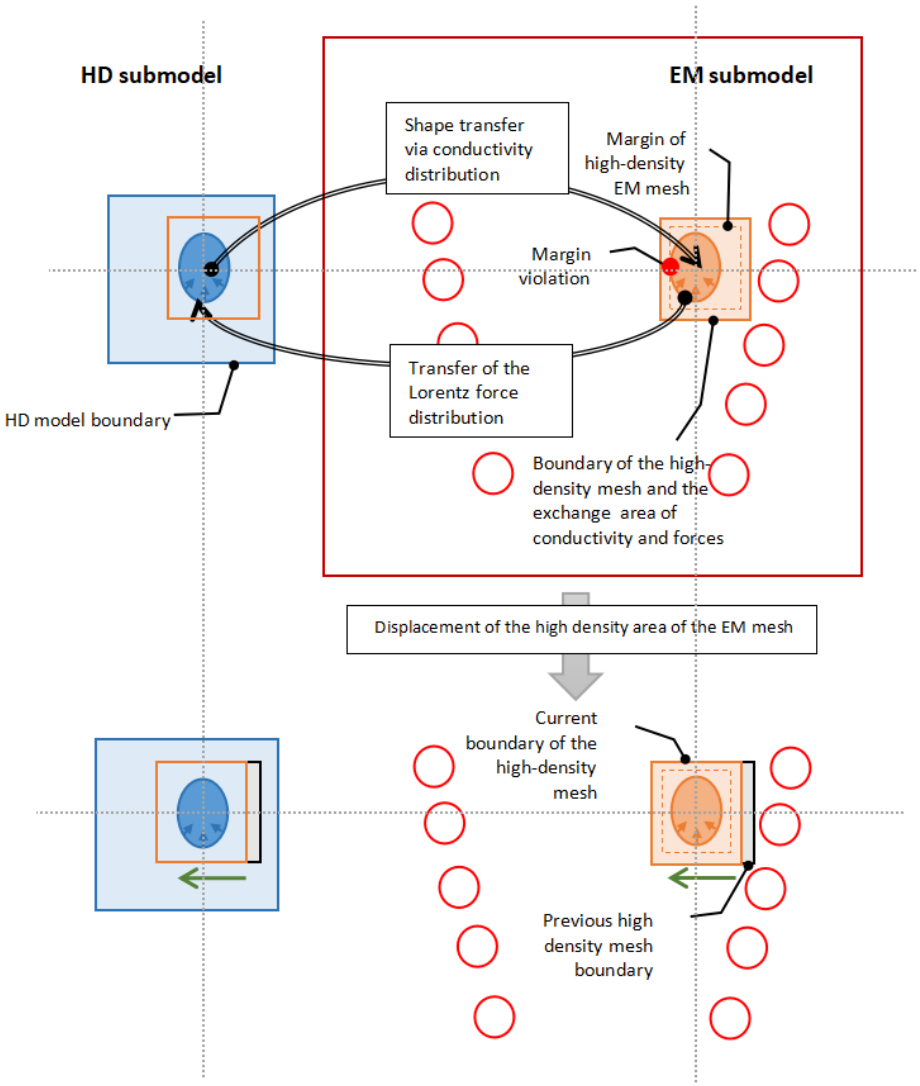

Figure 4: Simplified 2D visualization of displacement of the three-dimensional high-density EM mesh area (surrounding the metal bath) as a result of the metal entering the margin of this area: orange solid line - boundary area of high-density mesh, orange dashed line - detection line of margin violation, red dot - example of a margin violation, green arrow - direction of displacement of the high-density mesh area after the margin line is violated, black line with gray area - original location of the high-density area before the displacement, dotted gray lines - auxiliary lines showing the absolute position of the melted metal in both submodels and both simulation steps.

displacement is performed in 3D space because the developed model is a full 3D model. However, to improve readability, the idea of the method is presented in the form of a simplified 2D visualization in Fig. 4. The figure shows both computational domains working together: hydrodynamic (HD) and electromagnetic (EM). The total sizes of these domains are completely different. The common point of cooperation is the area of the model attention focused on the liquid bath. In this zone, the high-density EM mesh is consistent with the permanent, structured mesh of the HD model. Thanks to this, the conductivity distribution (from the HD submodel) and the Lorentz force and Joule heat distributions (from the EM submodel) can be exchanged between the submodels without interpolation.

In cases where the metal occupies a significantly smaller volume compared to the entire internal volume of the coil, and the system experiences negligible external atmospheric flow influence (as in the example below) or operates in a vacuum, the molten metal's hydrodynamics becomes localized. Its flow distribution and shape are not influenced by factors other than the Lorentz forces acting directly on it. This localization allows the hydrodynamic model to be restricted to analyzing only the metal's immediate surroundings, resulting in faster computational times for the hydrodynamic submodel. Therefore, as shown in Fig. 5, the developed simulation system also includes a second, parallel attention mechanism for the HD submodel. The mechanism for detecting the need to shift the HD domain is again based on detecting margins (Fig. 6). If the attention area of the EM model (the high-density mesh area marked with the orange line) enters the margin zone of the HD domian (the blue dashed line), the entire domain is moved toward this margin. Numerically, this is accomplished by shifting in the opposite direction distributions of all variables tracked in this submodel (velocity, pressure, turbulence, energy). The use of a structural mesh with cuboid, identical cells in the HD submodel makes this operation trivial. In the case of the HD submodel, the computational domain is large enough that there is no need to change its size as a result of a deformation of the metal load. During the shift of the HD domain, the absolute position in space of the attention region of the EM model does not change.

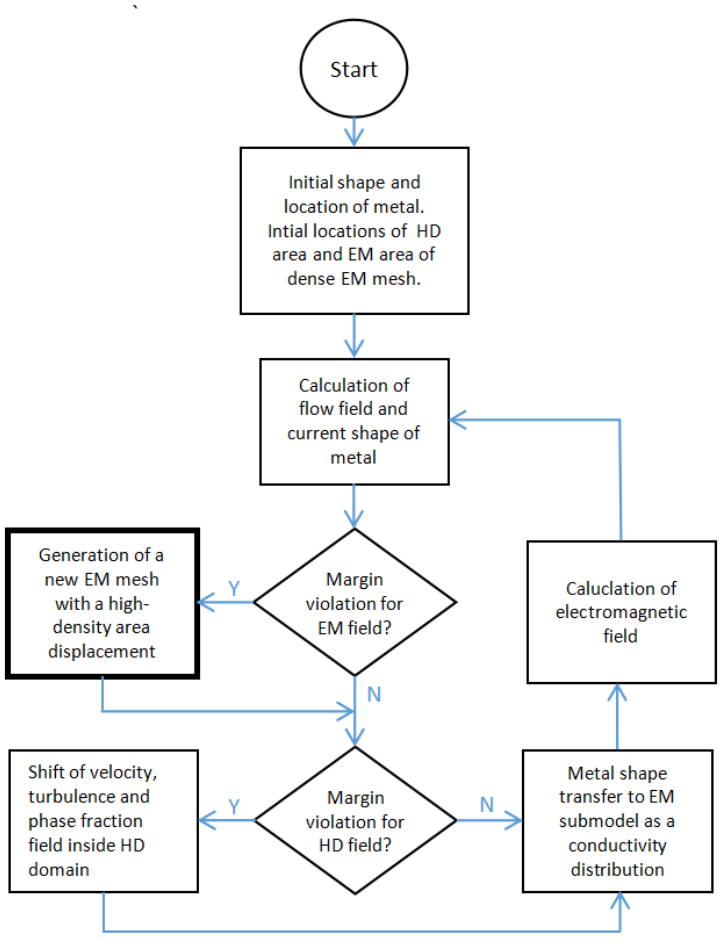

Figure 5: Displacements of attention areas in the HD and EM submodels

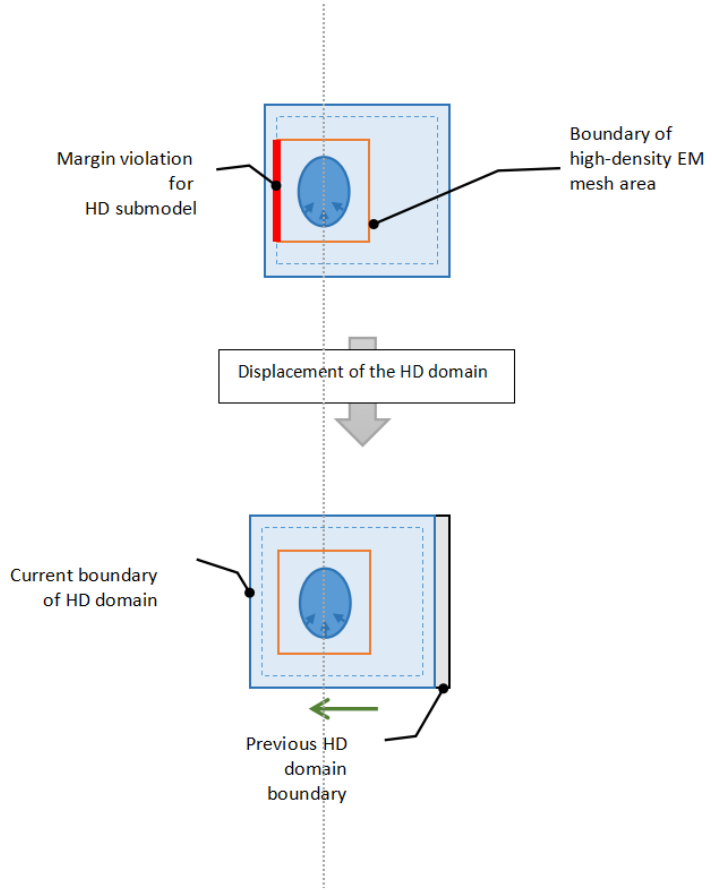

Figure 6: Simplified 2D visualization of displacement of the three-dimensional HD domain as a result of the metal exceeding the margin of this area: blue solid line - boundary area of HD domain, blue dashed line - detection line of margin violation, orange solid line - boundary of the EM model attention area (the high-density EM mesh), red solid line - example of a margin violation, green arrow - direction of displacement of the HD domain after the margin line is violated, black line with gray area - original location of the HD domain before the displacement, dotted gray line - auxiliary line showing the absolute position of the melted metal and the high-density EM mesh area (the attention area of the EM model) in both simulation steps.

2.1. Mathematical description of the EM submodel

The model implemented in GetDP software is based on an approach using the magnetic vector potential $\mathbf{A}$ solved in the frequency domain:

$$\nabla \times \left(\frac{1}{\mu} \nabla \times \mathbf{A} \right) + j\omega\sigma\mathbf{A} = \mathbf{J}_s \tag{2}$$

where μ is the magnetic permeability, σ is the electric conductivity, ω is the angular frequency and $\mathbf{J}_s$ is the current density source.

Electrical conductivity σ, depending on the domain zone, can be uniform (for the coil and ambient air) or non-uniform (to describe the shape of the liquid metal).

Based on the spatial distribution of the magnetic potential $\mathbf{A}$, we can determine the distribution of induction $\mathbf{B}$ (3) and induced current density $\mathbf{J}$ (4):

$$\mathbf{B} = \nabla \times \mathbf{A}, \tag{3}$$

$$\mathbf{J} = -j\omega\sigma\mathbf{A}. \tag{4}$$

The above two quantities will allow us to determine the time-averaged distribution of Lorentz electromagnetic forces $\mathbf{f}_{\mathrm{EL}}$ (5) and Joule heat sources q_{J} (6) transferred to the hydrodynamic submodel:

$$\mathbf{f}_{\mathrm{EL}} = \frac{1}{2} \operatorname{Re} \left(\mathbf{J} \times \mathbf{B}^* \right) \mathbf{A}, \tag{5}$$

$$q_{\mathrm{J}} = \frac{1}{2} \frac{|\mathbf{J}|^2}{\sigma}, \tag{6}$$

where $\mathbf{B}^*$ is the complex conjugate of $\mathbf{B}$.

2.2. Mathematical description of the HD submodel

The hydrodynamic model (implemented in Ansys Fluent software) is based on the Navier–Stokes momentum conservation equation (7), in which one of the source term is the volume density of the Lorentz force $\mathbf{f}_{\mathrm{EL}}$ acting on the liquid metal, provided by the electromagnetic model:

$$\frac{\partial}{\partial t}(\rho\mathbf{v}) + \nabla(\rho\mathbf{v}\mathbf{v}) = -\nabla p + \eta_{eff}\nabla^2\mathbf{v} + \mathbf{f}_{\mathrm{EL}} + \mathbf{f}_{\mathrm{S}} + \rho\mathbf{g}, \tag{7}$$

where ρ is the fluid density, $\mathbf{v}$ is the fluid velocity, p is the pressure, η_{eff} is the effective viscosity determined from the k-ω turbulence model, $\mathbf{f}_{\mathrm{S}}$ is the surface tension and $\mathbf{g}$ is the gravity.

The flow within the levitation system was modeled as multiphase with a free surface. To simulate this process, the classic Volume of Fluid (VOF) [28] method was employed. To track the evolution of the molten metal's free surface, the volume fraction conservation equation for one of the phases was solved:

$$\frac{\partial}{\partial t}(\alpha_q \rho_q) + \nabla(\alpha_q \rho_q \mathbf{v}) = 0. \tag{8}$$

In the VOF approach, material properties which appear in the equation (the density ρ and viscosity η in Eq. 7) were determined based on the weighted average of volume fraction and property of each phase. After reconstructing the shape of the interface between liquid metal and air for the current phase share distribution by the VOF method, the surface tension is determined, which is an additional source term $\mathbf{f}_\mathrm{S}$ in equation (7). Surface tension modelling was implemented as the continuum surface force expressed as a body force in the momentum conservation equation using divergence theorem [29].

3. Experiment and results discussion

The developed hybrid model was tested on the example of a classic levitation melting system. The coil geometry was developed by the authors in previous research [30]. It is characterized by a standard change in the direction of the last and highest turn (Fig. 8). The aluminum load levitates near the axis of the system. Due to the high frequency (277 kHz) of the electromagnetic field, a high-density mesh ($<<$ 0.0005 mm) is required in the molten metal area. At the same time, the load occupies a very small volume inside the coil compared to the space of the possible presence of metal load inside the coil. Therefore, the developed hybrid model seems predisposed to modeling such a process. Data about the experimental setup are presented in Table 1. The properties of liquid aluminum were assumed to be those used in previous publications on aluminum levitation melting [31].

Table 2 shows the parameters of the numerical model used. The decision to re-calculate the preconditioner was based on the number of iterations of the GMRES method in the previous simulation step. If the number of iterations exceeded 30, the preconditioner was considered non-representative and was recalculated.

Parameter	Value
Metal load diameter (in the initial spherical shape)	6 mm
Turn diameter	6 mm
Density of molten aluminum	2380 kg/m^3
Surface tension of molten aluminium	0.94 N/m
Electrical conductivity of molten aluminium	3.8 MS/m
Electrical conductivity of the copper coil	58 MS/m

Table 1: Parameters of the experimental system

Parameter	Value
Number of tetrahedra of 3D mesh	∼800 thousand
HD cell size	0.00013 m
EM cell size	0.00013 m
Witdh, depth of the HD domain	0.013 m
Height of th HD domain	0.026 m
Margin width for the HD domain	0.0013 m
Size of EM high density zone	adaptive
Margin width for the EM high density zone	0.00026 m
Simulation time step	0.01 s
Relative convergence tolerance for GMRES method	1e-12
Iteration number threshold for preconditioning refresh	30

Table 2: Parameters of the numerical 3D model

Figure 7 shows exemplary simulation time step components for successive simulation steps during a period of high variability of the metal geometry. The adopted threshold of 30 iterations causes that only in every 5th step of the simulation in the EM submodel, in addition to the standard operations (GMRES iterations and postprocessing), the preconditioner was calculated. Thanks to this, our hybrid model allowed for an average reduction of the EM calculation time to 31 % of the time in which the precondioner would be determined at each time step, as is the case in previously developed models of electromagnetic levitation.

Figures 8 and 9 show the position and shape of the liquid metal (after the process has stabilized as a result of reaching a state of equilibrium between gravity, electromagnetic forces and surface tension) in the experiment and determined in the model. For the two analyzed coil supply currents (600 A and 650 A), satisfactory position and shape compliance was obtained. Of

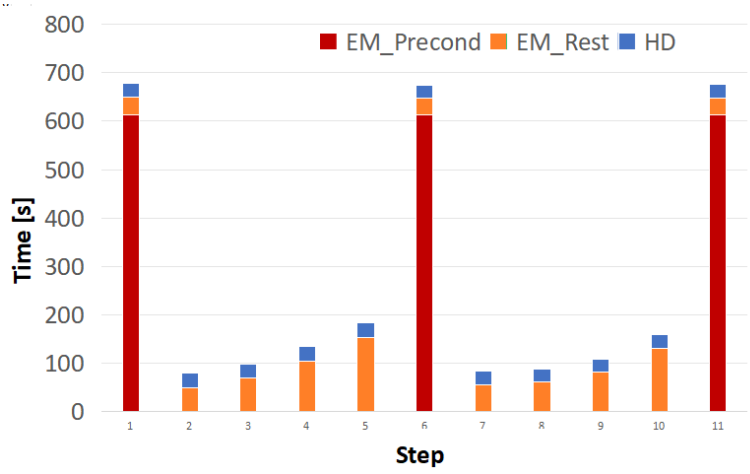

Figure 7: Time of the simulation time step components (after 1 second of simulation).

course, it should be taken into account that the difference in the scales of the load and the coil causes that even the smallest inaccuracies in the mapping of the coil geometry and its orientation in space relative to the direction of gravity causes noticeable differences in the location of the molten metal in the experiment and the numerical model. With the device being analyzed, such an error is inevitable. However, it should be noted that the phenomena of molten metal deformation and forced convection of liquid metal are local in nature and are not strongly dependent on the position of the metal load (of course, within a certain range of differences). This explains the better agreement observed in the shape compared to the position.

The numerical model allows us to analyze phenomena that cannot be measured in an experiment. Figure 10 shows the distribution of Lorentz forces on the surface of molten metal for two supply currents (and two equilibrium positions of the metal load). In both cases, the disappearance of forces in the axis of the metal load, typical of classic levitation melting, is visible. The central region of the metal is supported only by the limited surface tension forces of the liquid metal. Consequently, the classic levitation melting system is restricted to processing small molten loads. When dealing with larger masses, the hydrostatic pressure overcomes the resistance offered by surface tension [11]. A similar decay of the electromagnetic field can be seen in the case of Joule heat generated in the metal load (Fig. 11).

Figures 12 and 13 show a rather complex, asymmetrical distribution of

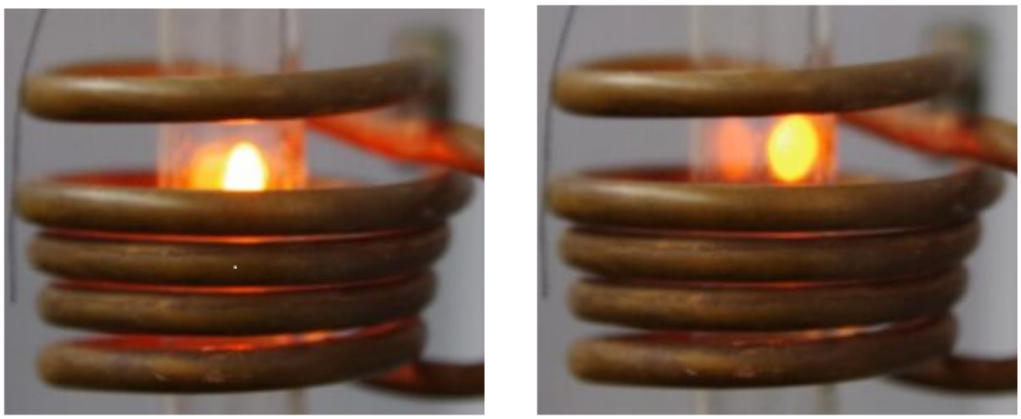

Figure 8: Molten metal load for a current of 600 A and 650 A.

flows in the molten metal loads. Interestingly, despite the different shapes and locations of the molten metal (for different supply currents), the structures of these flows are quite similar. The obtained flow velocities are low, but the small size of the molten metal load (6 millimeters in diameter for the original sphere) should be taken into account.

4. Conclusions

The paper proposes a hybrid levitation melting model, whose main idea is based on the use of data from previous simulation steps in the EM submodel. Thanks to the conditional refreshing of the preconditioner, the simulation time was reduced threefold compared to the models previously used in the analysis of electromagnetic levitation, in which the electromagnetic field is independently calculated for each step of the simulation. This applies to both models based on the generation of a new mesh in each step based on the approximation of the shape of the liquid metal, as well as models using shape transfer through conductivity distribution. Moreover, the developed methodology includes dynamic, adaptive focusing of the EM and HD submodels on the molten metal area.

Accelerating the process simulation increases the chances of introducing the model into a cycle of superior numerical optimization of the inductor

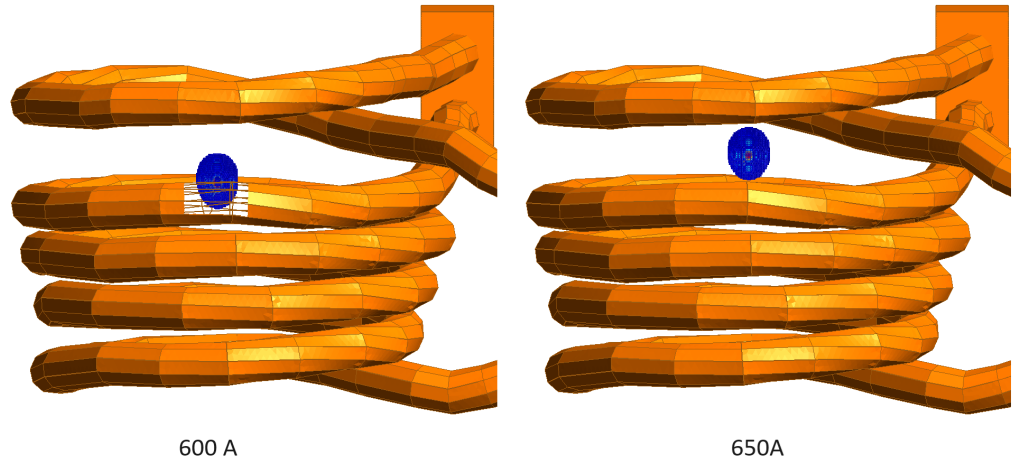

Figure 9: The shape of the metal in the three-dimensional EM submodel (GetDP) reproduced by the conductivity distribution for a current of 600 A and 650 A.

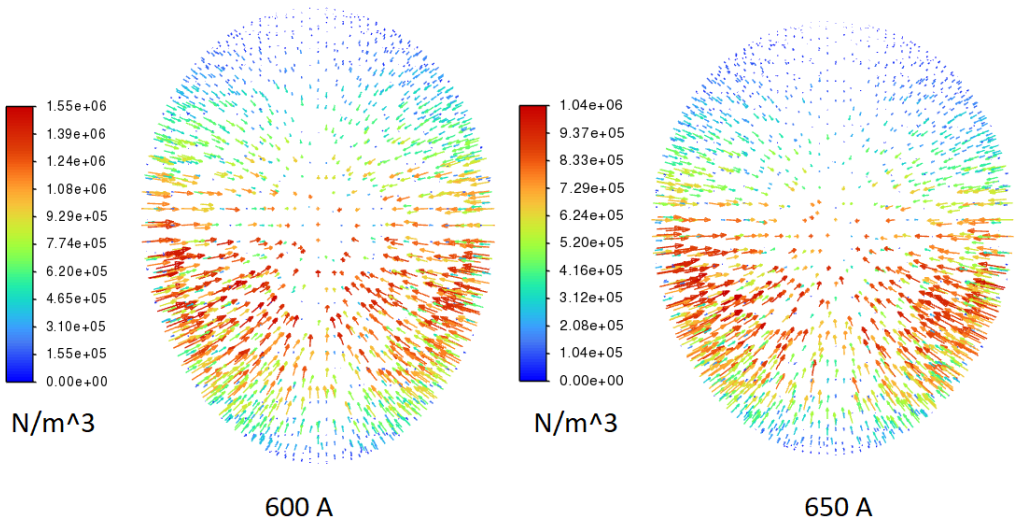

Figure 10: Distribution of Lorentz forces on the three-dimensional surface of the molten metal load for a current of 600 A and 650 A.

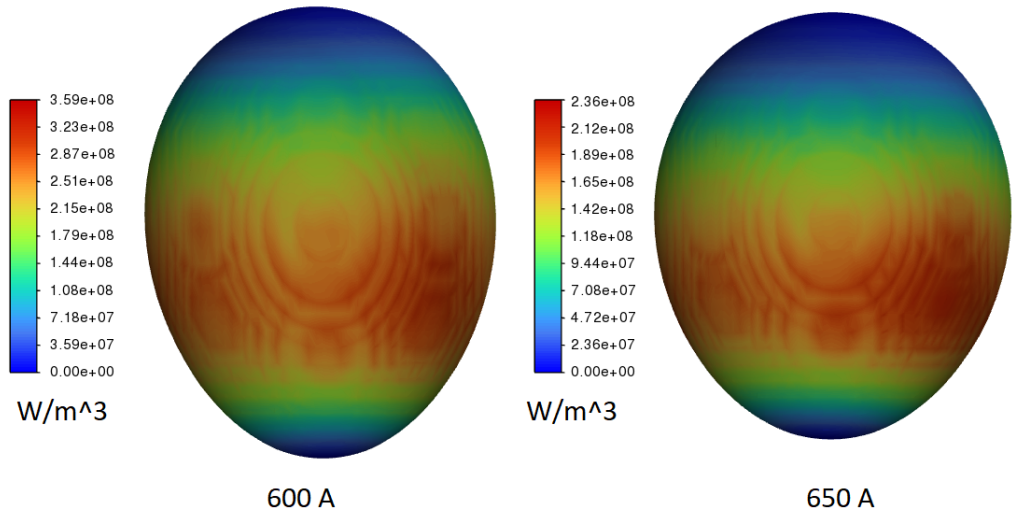

Figure 11: Distribution of Joule heat sources on the three-dimensional surface of the molten metal load for a current of 600 A and 650 A.

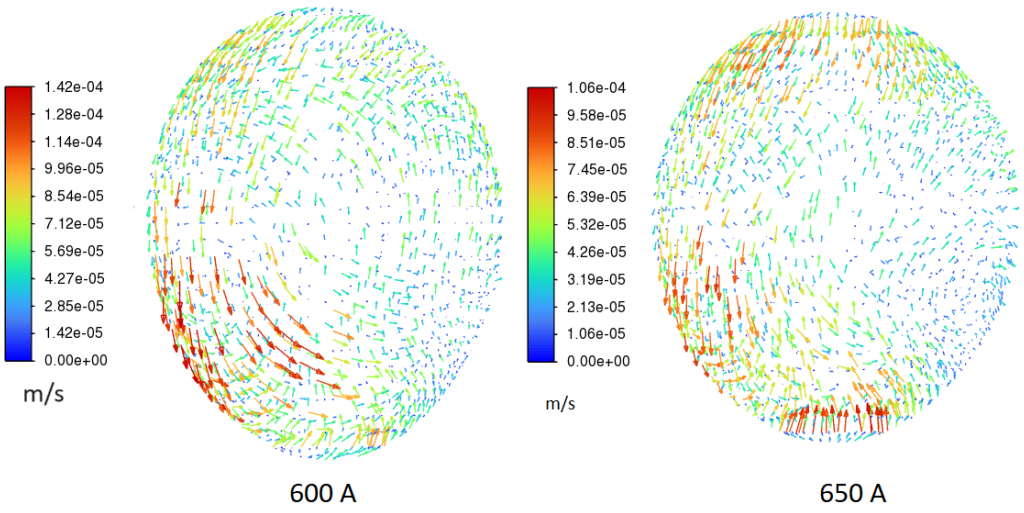

Figure 12: Velocity distribution on the three-dimensional surface of the molten metal load for a current of 600 A and 650 A.

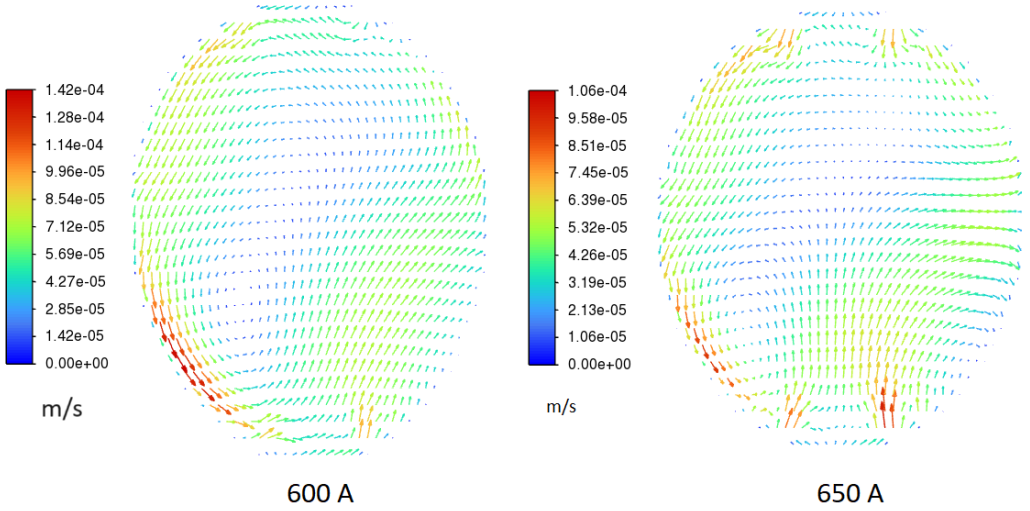

Figure 13: Velocity distribution over the 2D cross-section of the molten metal load for a current of 600 A and 650 A.

geometry and/or power supply parameters and improving existing solutions based on constant molten metal geometry [32].

The developed tool can be used not only for modeling levitation or semi-levitation melting (with a cold crucible), but also for any MHD processes with the presence of a variable free surface of liquid metal (e.g. melting in non-conductive crucibles, electromagnetic stirrers, metal casting in the presence of an EM field).

In the experimental implementation of the model, the decision to refresh the preconditioner was based on a simple, pre-selected threshold for the number of GMRES iterations . An interesting further development of the method may be to supplement it with an algorithm for optimizing the moment of the preconditioner refreshing, the aim of which will be to dynamically minimize the average calculation time for one simulation step.

Acknowledgements

Publication supported by the Excellence Initiative - Research University program implemented at the Silesian University of Technology, year 2024, grant no 11/040/SDU/10-21-02 (scientific internship of Sławomir Golak at the University of Liège under the supervision of Christophe Geuzaine).

References

[1] M. Palacz, B. Melka, B. Wecki, Siwiec, al., Experimental analysis of the aluminium melting process in industrial cold crucible furnaces, Metals and Materials International 26 (5) (2020) 695–707. doi:10.1007/s12540-019-00368-2.

[2] M. Guglielmi, E. Baake, A. Köppen, E. Holzmann, S. Herbst, S. M. Maryamnegari, Induction melting in a cold crucible furnace applied to innovative high-melting temperature metals, Magnetohydrodynamics 58 (4) (2022) 523–532.

[3] V. Bojarevics, T. Nishimura, D. Matsuwaka, Development of advanced cold crucible melting of titanium alloys, Magnetohydrodynamics 58 (1) (2022) 13–24. doi:doi:https://doi.org/10.22364/mhd.

[4] R. Sabouni Tabari, M. Halali, A. Javadi, M. Khanjanpour, Experimental analysis and characterization of high-purity aluminum nanoparticles (al-nps) by electromagnetic levitation gas condensation (elgc), Nanomaterials (Basel) (2020). doi:10.3390/nano10102084.

[5] J. P. Witteveen, M. A. B. Vrielink, R. van Gastel, A. van Houselt, H. J. W. Zandvliet, Containerless metal single-crystal growth via electromagnetic levitation, Review of Scientific Instruments 92 (10) (2021). doi:10.1063/5.0064486.

[6] B. Friedrich, J. Morscheiser, C. Lochbichler, Potential of ceramic crucibles for melting of titanium alloys and gamma-titaniumaluminide, 51. Internationales Feuerfestkolloquium, At: Aachen/Germany (2008). doi:10.13140/RG.2.1.2084.0562.

[7] S. Schafföner, C. G. Aneziris, H. Berek, J. Hubálková, B. Rotmann, B. Friedrich, Corrosion behavior of calcium zirconate refractories in contact with titanium aluminide melts, Journal of the European Ceramic Society 35 (3) (2015) 1097–1106. doi:https://doi.org/10.1016/j.jeurceramsoc.2014.09.032.

[8] S. Fashu, M. Lototskyy, M. W. Davids, L. Pickering, V. Linkov, S. Tai, T. Renheng, X. Fangming, P. V. Fursikov, B. P. Tarasov, A review on crucibles for induction melting of titanium alloys, Materials Design 186 (2020) 108295. doi:https://doi.org/10.1016/j.matdes.2019.108295.

[9] S. Spitans, E. Baake, A. Jakovics, H. Franz, Large scale electromagnetic levitation melting of metals, International journal of applied electromagnetics and mechanics 53 (1) (2017) S61–S66, hES Conference, Padua Univ, Padua, ITALY, MAY 24-27, 2016. doi:10.3233/JAE-162238.

[10] S. Spitans, H. Franz, E. Baake, A. Jakovics, Large-scale levitation melting and casting of titanium alloys, Magnetohydrodynamics 53 (4, SI) (2017) 633–641, 8th International Scientific Colloquium on Modelling for Materials Processing (MMP), Riga, LATVIA, SEP 21-22, 2017. doi:10.22364/mhd.53.4.5.

[11] S. Golak, B. Panic, Numerical model of large-scale levitation melting process, Archives of metallurgy and materials 64 (2) (2019) 627–632. doi:10.24425/amm.2019.127590.

[12] R. Chen, Y. Yang, H. Fang, Y. Yang, Q. Wang, J. Guo, H. Ding, Y. Su, H. Fu, Glass melting inside electromagnetic cold crucible using induction skull melting technology, Applied Thermal Engineering 121 (2017) 146–152. doi:10.1016/j.applthermaleng.2017.04.050.

[13] P. Bulinski, J. Smolka, S. Golak, R. Przylucki, M. Palacz, G. Siwiec, J. Lipart, R. Bialecki, L. Blacha, Numerical and experimental investigation of heat transfer process in electromagnetically driven flow within a vacuum induction furnace, Applied Thermal Engineering 124 (2017) 1003–1013. doi:10.1016/j.applthermaleng.2017.06.099.

[14] P. Bulinski, J. Smolka, S. Golak, R. Przylucki, et., Numerical modelling of multiphase flow and heat transfer within an induction skull melting furnace, International Journal of Heat and Mass Transfer 126 (B) (2018) 980–992. doi:10.1016/j.ijheatmasstransfer.2018.06.074.

[15] P. Bulinski, J. Smolka, G. Siwiec, L. Blacha, S. Golak, R. Przylucki, M. Palacz, B. Melka, Numerical examination of the evaporation process within a vacuum induction furnace with a comparison to experimental results, Applied Thermal Engineering 150 (2019) 348–358. doi:10.1016/j.applthermaleng.2019.01.008.

[16] P. Bulinski, J. Smolka, S. Golak, R. Przyłucki, et., Analysis of al-zn alloy refining in an industrial induction skull melter with two crucible types,

International Journal of Heat and Mass Transfer 179 (2021) 121704. doi:10.1016/j.ijheatmasstransfer.2021.121704.

[17] C. Zhang, F. Cao, L. Zhang, Z. Jin, G. Cao, Z. Qiu, H. Shen, Y. Huang, S. Jiang, J. Sun, Break the superheat temperature limitation of induction skull melting technology, Applied Thermal Engineering 220 (2023). doi:10.1016/j.applthermaleng.2022.119780.

[18] P. Garcia-Michelena, E. Ruiz-Reina, N. Herrero-Dorca, X. Chamorro, Multiphysics modeling and experimental validation of heat and mass transfer for the vacuum induction melting process, Applied Thermal Engineering 243 (APR 15 2024). doi:10.1016/j.applthermaleng.2024.122562.

[19] J. Barglik, S. Golak, Modelling of filling a mold with molten metal in the presence of an electromagnetic field, Magnetohydrodynamics 51 (1) (2015) 5–14. doi:10.22364/mhd.51.1.2.

[20] X. Cai, H. Wang, B. Wei, Migration dynamics for liquid/solid interface during levitation melting of metallic materials, International Journal of Heat and Mass Transfer 151 (2020) 119386. doi:https://doi.org/10.1016/j.ijheatmasstransfer.2020.119386.

[21] S. Spitans, A. Jakovics, E. Baake, B. Nacke, Numerical modelling of free surface dynamics of melt in an alternate electromagnetic field, Magnetohydrodynamics 47(4) (2011) 385–397.

[22] J. Vencels, A. Jakovics, V. Geza, Simulation of 3d mhd with free surface using open-source eof-library: levitating liquid metal in an alternating electromagnetic field, Magnetohydrodynamics 53 (4) (2017) 643–652.

[23] S. Spitans, A. Jakovics, E. Baake, B. Nacke, Numerical modeling of free surface dynamics of melt in an alternate electromagnetic field: Part I. Implementation and verification of model, Metallurgical and Materials Transactions B 44 (2013) 593–605. doi:10.1007/s11663-013-9809-9.

[24] P. Dular, C. Geuzaine, GetDP reference manual: the documentation for GetDP, a general environment for the treatment of discrete problems, `http://getdp.info`.

[25] C. Geuzaine, GetDP: a general finite-element solver for the de Rham complex, in: PAMM Volume 7 Issue 1. Special Issue: Sixth International Congress on Industrial Applied Mathematics (ICIAM07) and GAMM Annual Meeting, Zürich 2007, Vol. 7, Wiley, 2008, pp. 1010603–1010604.

[26] C. Geuzaine, J.-F. Remacle, Gmsh: A 3-d finite element mesh generator with built-in pre- and post-processing facilities, International Journal for Numerical Methods in Engineering 79 (11) (2009) 1309–1331. doi:https://doi.org/10.1002/nme.2579.

[27] Y. Saad, M. H. Schultz, Gmres: A generalized minimal residual algorithm for solving nonsymmetric linear systems, SIAM Journal on Scientific and Statistical Computing 7 (3) (1986) 856–869. doi:10.1137/0907058.

[28] C. Hirt, B. Nichols, Volume of fluid (VOF) method for the dynamics of free boundaries, Journal of Computational Physics 39 (1) (1981) 201–225. doi:https://doi.org/10.1016/0021-9991(81)90145-5.

[29] J. Brackbill, D. Kothe, C. Zemach, A continuum method for modeling surface tension, Journal of Computational Physics 100 (2) (1992) 335–354. doi:https://doi.org/10.1016/0021-9991(92)90240-Y.

[30] B. Nycz, R. Przyłucki, Maliński, Comparison of characteristics for two selected inductors for levitation melting, in: 2023 14th International Conference on Measurement, 2023, pp. 222–225. doi:10.23919/MEASUREMENT59122.2023.10164580.

[31] S. Spitans, E. Baake, B. Nacke, A. Jakovics, Numerical modeling of free surface dynamics of melt in an alternate electromagnetic field. part ii: Conventional electromagnetic levitation, Metallurgical and Materials Transactions B 47 (1) (2016) 522–536. doi:10.1007/s11663-015-0515-7.

[32] B. Nycz, R. Przylucki, L. Malinski, S. Golak, Optimization of an inductor for electromagnetic levitation melting, COMPEL - The International Journal for Computation and Mathematics in Electrical and Electronic Engineering (2024). doi:10.1108/COMPEL-06-2023-0233.